Advanced Steel Construction – Vol. 21 No. 6 (2025) 511–519
DOI:10.18057/IJASC.2025.21.6.4

DYNAMIC RESPONSES OF HIGH-STRENGTH CONCRETE-FILLED HIGH-STRENGTH SQUARE STEEL TUBULAR COLUMNS UNDER VEHICLE COLLISION

Guo-Chang Li, Run-Ze Liu *, Xiao Li, Jia-Long Wang and Yue Zhou

School of Civil Engineering, Shenyang Jianzhu University, Shenyang, Liaoning 110168, China
** (Corresponding author: E-mail: runzeliu1996@163.com)*

ABSTRACT

High-strength concrete-filled high-strength square steel tubular (HCFHST) columns are vital structural elements in modern constructions, such as high-rise and large-span structures, due to their superior strength and reliability. However, during their services, they face challenges from vehicle collisions, which can compromise structural safety. To better understand their dynamic behaviours under vehicle collisions, dynamic constitutive relations for high-strength materials at high strain rates have been verified, firstly. Then, based on the verified simulation model, the working mechanisms of HSCFST columns under truck collision, including internal force development, damage evolution, and energy-dissipation mechanisms, are revealed. Furthermore, the influence of sectional dimensions, steel tube thickness, column height, axial compression ratio, material strengths, vehicle weight, and collision velocity on the anti-collision performance of HSCFST columns is presented. Simulation results indicate that HCFHST columns experience flexural deformation during collisions, and the cargo impact stage is the primary stage for plastic deformation development. The greatest bending moment occurs at the bottom, while the greatest shear force appears at the impact height. As deformation progresses, the steel tube becomes a critical internal force bearing component. The collision velocity, vehicle weight, sectional dimensions, steel tube thickness and steel strength are key factors affecting the anti-collision performance and energy-dissipating capacity of the HCFHST columns. By selecting key parameters according to the parametric study results, the maximum displacement calculation formula for HCFHST columns using the equivalent single degree of freedom method has been established, laying a foundation for the anti-collision design of HCFHST columns.

ARTICLE HISTORY

Received: 10 May 2025
Revised: 11 June 2025
Accepted: 12 June 2025

KEYWORDS

Concrete-Filled Steel Tubular Columns;
High-Strength Materials;
Dynamic Constitutive Relations of Materials;
Vehicle Collisions;
Dynamic Responses

1. Introduction

Modern transportation means have become an indispensable component of people's lives. Traffic safety issues like vehicle collisions are not infrequent and have attracted extensive attention. When a vehicle collides with a building, the consequences are likely significant, with the potential for substantial damage or even structural collapse, resulting in many casualties and property losses. Consequently, impact loads have emerged as a primary concern within civil engineering. Current standards in different countries [1-4] apply the equivalent static method for the anti-impact design, with the basic principle of applying a static load at the collision height. However, this method cannot properly reflect the dynamic behaviour of components to meet the safe requirements and reasonable design. It fails to cover the effect of various parameters on the dynamic response of components and underestimates the damage caused by large trucks and comparable vehicles. Consequently, the revelation of the working mechanisms and dynamic responses of components or structures can facilitate their precise design.

The extensive utilization of high-strength concrete-filled high-strength steel tubular (HCFHST) components in large-span and high-rise structures can be attributed to their high bearing capacity, good ductility, lightweight nature, and compact cross-sectional dimensions [5]. Consequently, researchers have examined the anti-impact behaviour and failure mechanism of HCFHST members through experimental research, numerical simulation, theoretical analysis, and other research methodologies. As demonstrated by Han et al. [6], high-strength concrete-filled steel tubular (HCFST) components exhibit superior toughness and impact resistance in transverse impact tests. Furthermore, a dynamic increase factor expression for the flexural capacity of HCFST components has been proposed, considering steel strengths, steel ratios, cross-sectional dimensions, and impact velocities. Hou et al. [7] have discovered that, due to the distinctive dynamic mechanical properties exhibited by high-strength steel, the impact resistance of CFHSST components is reduced when subjected to high-energy impact conditions in comparison with that of ordinary CFST components. Consequently, it was determined that CFHSST components may manifest evident performance deficiencies when exposed to extreme conditions. Yang et al. [8,9] have revealed the typical dynamic behaviours, loading mechanism, and residual properties of square HCFHST components under lateral impact with axial compression. A m-v-n failure criterion for HCFHST components has been put forward, and the calculation formulas for lateral impact bearing capacity and the maximum displacement calculation were proposed Li et al. [10] demonstrated that HCFHST columns show flexural deformation under impact loads and exhibit excellent impact resistance, as confirmed by a lateral impact test. Additionally, a formula for calculating the energy-dissipating coefficient for columns has been established. In the impact test on HCFHST columns, the aforementioned scholars employed rigid trolleys as a substitute for vehicles, thus neglecting the deformation and damage incurred by vehicles. Moreover, the impact mass and velocity in the aforementioned literature are comparatively minor in terms of vehicle collision, thus rendering it unfeasible to undertake a thorough investigation of the failure modes of the HCFHST columns under vehicle collision through the impact test. Consequently, the information for anti-collision design for the HCFHST column is still limited. Furthermore, due to the elevated expense and protracted duration of full-scale vehicle impact tests, there is currently a lack of experimental research on the dynamic performance of full-scale HCFHST columns in vehicle collisions.

Concerning vehicle impact loads, scholars have focused their research on the dynamic performance of reinforced concrete (RC) piers. However, there are comparatively few numerical simulations on concrete-filled steel tubular (CFST) columns. Saini et al. [11] have verified the feasibility of replacing RC piers with CFST piers through a comparison of the dynamic behaviours of those piers under impact loads. Furthermore, the influence of the key design parameters of CFST piers has been revealed, and the improvement directions of the impact resistance design of CFST piers have been identified. Alam et al. [12] have established a simplified rigid-body-spring model to simulate the vehicle impact of a Chevrolet C2500 truck on full-scale CFST components and those reinforced with CFRP. By comparing the dynamic behaviours with or without the simplified model, it is necessary to consider the vehicle deformation. Yu et al. [13] conducted a study of the dynamic behaviours of CFRP-reinforced CFST columns and CFRP-reinforced hollow steel tubes under vehicle impacts. The findings indicated that CFRP-reinforced CFST columns exhibit superior impact resistance in comparison to CFRP-reinforced hollow steel tubes. Hu et al. [14] have conducted a study on the mechanical properties of CFST piers when subjected to vehicle impacts. An evaluation of CFST piers has been conducted by the United States, European, and Chinese standards, and the applicable scopes of these standards have also been determined. In subsequent research, Hu et al. [15] found that the ratio of the mid-span residual displacement to the column height can be used as an effective index for evaluating the remaining bearing capacity of the CFST columns. Consequently, a prediction model for residual deformation has been formulated. Therefore, by drawing on the research achievements of domestic and foreign scholars on reinforced concrete piers under vehicle impacts, the present paper will examine the anti-collision behaviour of HCFHST columns under vehicle collision.

In this paper, LS-DYNA is employed to analyse the anti-collision behaviours and working mechanisms of HCFHST columns under vehicle collisions. Furthermore, the impacts of parameters, including sectional dimensions, steel tube thickness, column height, axial compression ratio, material strengths, vehicle weight, and impact velocity on the anti-collision performance of HCFHST columns are revealed. A maximum displacement calculation formula of HCFHST columns under vehicle collision is proposed to guide the engineering practice.

2. Modelling of finite element (FE) models

2.1. Modelling

The FE models of the HCFHST column collide with the truck are built with LS-DYNA, as illustrated in Fig. 1. As stated in reference [10], the *CONTACT_AUTOMATIC_SURFACE_TO_SURFACE and *CONTACT_TIED_SURFACE_TO_SURFACE algorithms are chosen to represent the contact within steel and concrete and the contact between steel and steel, respectively. The friction coefficient of the steel-concrete interface and steel-steel interface is taken as 0.6 and 0.15, respectively. To guarantee the accuracy of the simulated results, the Ford F800 SUT developed by NCAC and FHWA was used, which is available at https://thyme.ornl.gov/FHWA/F800WebPage/description/desc2.html. The model can accurately simulate truck-infrastructure interactions under impact, failure modes of the vehicle and post-crash vehicle stability [11,15].

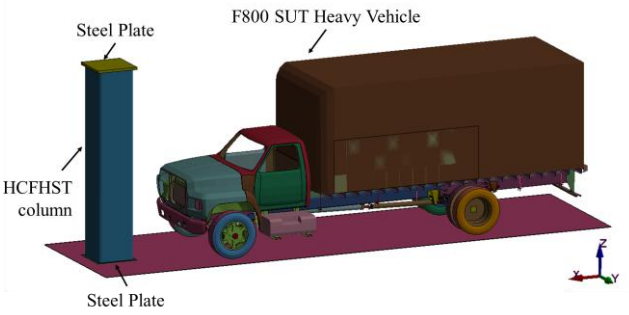

Fig. 1 Established FE model

2.2. Constitutive relations of materials

2.2.1. Selection of constitutive relations for high-strength steel (HSS)

The *MAT_024 is selected to perform the behaviour of HSS [10], with the defined constitutive relation illustrated in Eq. (1). As stated in reference [15], the relationship between yield strength (f_y) and ultimate tensile strength (f_u) has been defined. Meanwhile, the CS model is selected to consider the strain rate effect, and the calculation formula is shown in Eq. (2) [17]. To further confirm the precision and applicability of the CS model and its material parameters, a total of 84 sets of experimental data were collected [18-27], covering a range of steel yield strengths from 420 to 1,000 MPa, and a range of strain rate variations from 0.0002 to 5,293 s^{-1}. The comparison of the collected test data with the calculation results of Eq. (2) is demonstrated in Fig. 2. As exhibited in Fig. 2, the data are distributed close to the prediction line of Eq. (2). The mean, standard deviation (SD) and coefficient of variation (CoV) of the ratio of the calculated DIF to the measured DIF is 0.90, 0.104 and 0.115, respectively. As demonstrated in Fig. 2, the CS model, with material constants of C=6844s^{-1} and p=3.91, is capable of accurately reflecting the mechanical properties of HSS, with a yield strength ranging within 420~1000 MPa and a strain rate ranging within 0.0002~5293 s^{-1}.

$$\sigma = \begin{cases} E_s\varepsilon & (\sigma \le f_y) \\ f_y + 0.01E_s(\varepsilon - \varepsilon_y) & (f_y < \sigma) \end{cases} \tag{1}$$

$$DIF = 1 + (\frac{\dot{\varepsilon}}{C})^{1/p} \tag{2}$$

where, $\dot{\varepsilon}$ is the strain rate; and C and p are material constants.

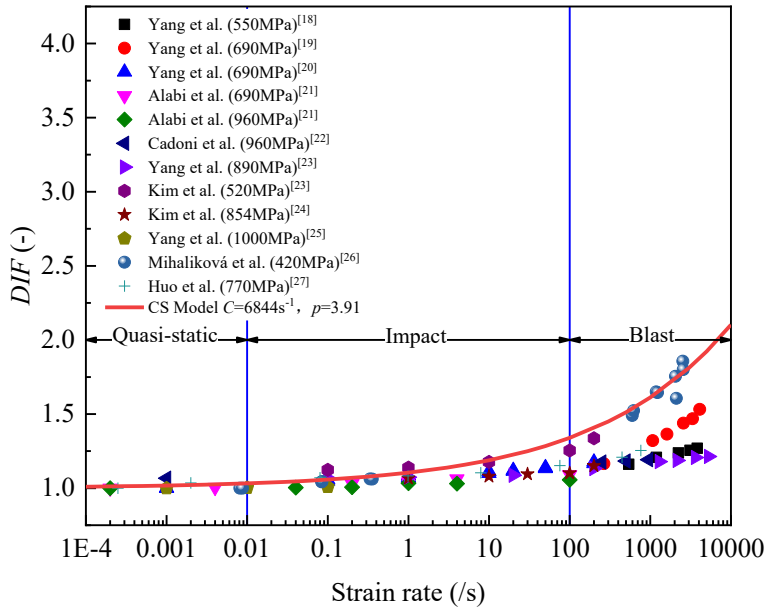

Fig. 2 Verification of the accuracy of CS strain rate model for HSS

2.2.2. Selection of constitutive relations for high-strength concrete (HSC)

The *MAT_72R3 is selected to represent the mechanical properties of high-strength concrete under triaxial compression. The DIF calculation formulas in European specification CEB-FIP (2010) are adopted to reflect the strain rate effect of HSC [28]. The calculation formula of DIF under compression and tension are displayed in Eqs. (3) and (4), respectively. To prove the precision and applicability of the DIF calculation formula, 72 sets of experimental data under dynamic compression [29-33] and 115 sets of experimental data under dynamic tension [34-36] are collected, covering compressive strength ranging within 60~120 MPa. Furthermore, the strain rate variations under dynamic compression and dynamic tension are in the ranges of 0.005~496 s^{-1} and 0.0005~175 s^{-1}, respectively. The collected results were compared with the calculated results of Eqs. (3) and (4), as shown in Fig. 3. The mean, SD, and CoV of the ratio of DIF calculated by Eq. (3) and Eq. (4) to the experimentally measured values are 0.97 and 0.89, 0.204 and 0.356, and 0.211 and 0.398, respectively. This indicates that the DIF calculation formula proposed by CEB-FIP (2010) can accurately reflect the mechanical behaviours of HSC with medium and high strain rates.

$$DIF_{compressive} = \begin{cases} (\dot{\varepsilon}_c/\dot{\varepsilon}_{c0})^{0.014} & \dot{\varepsilon}_c \le 30s^{-1} \\ 0.012(\dot{\varepsilon}_c/\dot{\varepsilon}_{c0})^{1/3} & \dot{\varepsilon}_c > 30s^{-1} \end{cases} \tag{3}$$

$$DIF_{tensile} = \begin{cases} (\dot{\varepsilon}_{ct}/\dot{\varepsilon}_{cto})^{0.018} & \dot{\varepsilon}_{ct} \le 10s^{-1} \\ 0.0062(\dot{\varepsilon}_{ct}/\dot{\varepsilon}_{cto})^{1/3} & \dot{\varepsilon}_{ct} > 10s^{-1} \end{cases} \tag{4}$$

where, $\dot{\varepsilon}_c$ and $\dot{\varepsilon}_{ct}$ are strain rate under compression and tension, respectively; $\dot{\varepsilon}_{c0} = 30 \times 10^{-6}\ s^{-1}$; and $\dot{\varepsilon}_{cto} = 1 \times 10^{-6}\ s^{-1}$.

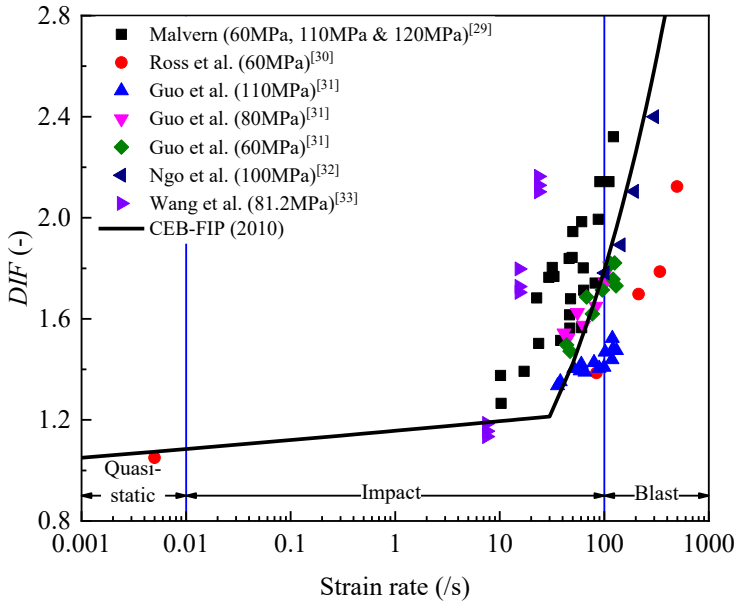

(a) HSC under compression

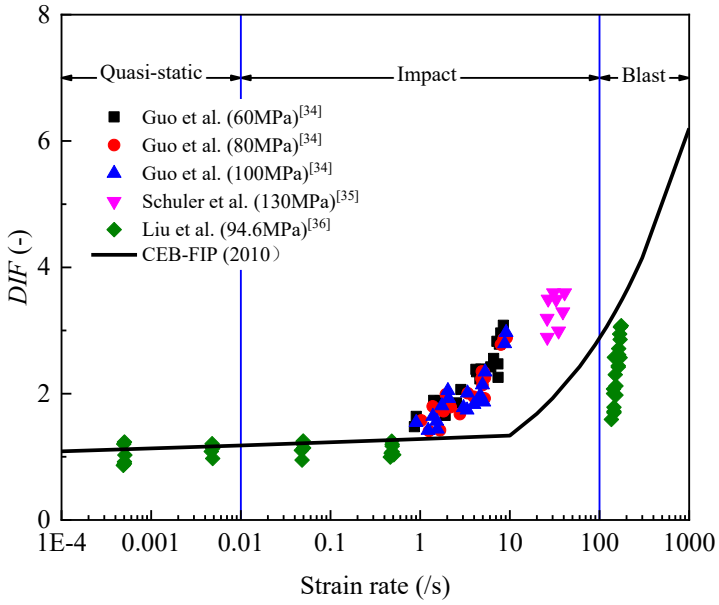

(b) HSC under tension

Fig. 3 Verification of the accuracy of DIF calculation formula for HSC

2.3. Model matrix

In this study, FE models are built to analyse the dynamic behaviours of HCFHST columns under various parameters. A total of 36 full-scale models of HCFHST columns, subjected to vehicle collision, have been established with differing parameters, which are detailed in Table 1.

3. Working mechanisms

To analyse the working mechanism of the typical column, the collision process, development of internal force, evolution of damage, and the energy dissipation mechanism are analysed.

3.1. Collision process

The impact force time-history curve is displayed in Fig. 4(a), and the displacement time-history curve is presented in Fig. 4(b). According to Fig. 4(a), the entire vehicle impact process can be divided into four stages as shown below.

Bumper impact stage (230~249 ms): In the initial collision stage, the bumper contacts the HCFHST column, with a collision height ranging between 520 and 1860 mm. This stage constitutes 18% of the total duration. The overall impact force is minor, exhibiting an increase followed by a subsequent decrease. Since the bumper stiffness is considerably lower than that of the HCFHST column, the impact force achieves its first peak of $0.01F_{max}$ at 238 ms, where F_{max} is the maximum impact force throughout the collision process. Subsequently, the impact force gradually attenuates due to the yield of the bumper. In this phase, the column's displacement is limited, with a displacement of $0.02u_{max}$, where u_{max} denotes the maximum displacement throughout the entire collision process.

Engine impact stage (249~265 ms): The engine has been found to undergo a secondary collision with the bumper as a result of inertia, with the effective collision height extending to 300~1890 mm. The duration of this stage constitutes 15% of the entire collision process. Since the engine exhibits greater stiffness than the bumper, the impact force and column deformation are increased to a greater extent than in the preceding stage. The impact force arrives a peak of $0.06F_{max}$ at 255 ms, and the displacement of the HCFHST column develops to $0.05u_{max}$ at 260 ms, although this remains constrained.

Cockpit impact stage (265~325 ms): The cockpit contacts with the HCFHST column, and the collision height is further extended to 300~2280 mm. This stage occupies 56% of the total duration. Due to the significant difference in stiffness between the cockpit and the HCFHST column, the cockpit is eventually completely crushed. Consequently, the impact force is insignificant at this stage, and its value is stable around $0.01F_{max}$. Furthermore, the displacement of the HCFHST column exhibits stability, with a maximum value of $0.02u_{max}$. It is noticed that the displacement and impact force of the HCFHST column do not significantly change at this stage.

Cargo impact phase (325~337 ms): The cargo container continues to move along the x-axis under the action of inertial force, and its collision range extends to 300~3460 mm. This stage constitutes 11% of the total duration. The trajectory of the cargo in the cargo container has been deflected due to constraints imposed by the residual structure of the cockpit. The collision between the cargo and the HCFHST column occurred at an angle of 2° to the x-axis, with the impact load primarily concentrated at a height of 2240 mm. As the stiffnesses of the cargo and HCFHST are close, the impact force reaches its maximum of 157,902 kN at 326ms. Subsequently, the displacement reaches a peak of 65 mm at 334ms. Then, once the kinetic energy of the cargo is depleted, the impact force gradually decreases to 0 kN, leading to a displacement of 36 mm for the HCFHST column, accompanied by a rebound rate of 55%. It has been determined that this stage represents the main deformation development stage of the HCFHST column under vehicle collision.

Table 1
Key model parameters and simulation results

No.	B (mm)	t (mm)	L (mm)	α (-)	n (-)	f_y (MPa)	f_{cu} (MPa)	m (ton)	v (m/s)	E (kJ)
C1	750	25	3900	12.9%	0.30	890	110	12000	33.3	6667
C2	750	25	3900	12.9%	0.30	770	110	12000	33.3	6667
C3	750	25	3900	12.9%	0.30	690	110	12000	33.3	6667
C4	750	25	3900	12.9%	0.30	620	110	12000	33.3	6667
C5	750	25	3900	12.9%	0.30	550	110	12000	33.3	6667
C6	750	25	3900	12.9%	0.30	460	110	12000	33.3	6667
C7	750	25	3900	12.9%	0.30	890	120	12000	33.3	6667
C8	750	25	3900	12.9%	0.30	890	100	12000	33.3	6667
C9	750	25	3900	12.9%	0.30	890	90	12000	33.3	6667
C10	750	25	3900	12.9%	0.30	890	80	12000	33.3	6667
C11	750	25	3900	12.9%	0.30	890	70	12000	33.3	6667
C12	750	25	3900	12.9%	0.30	890	60	12000	33.3	6667
C13	750	25	4200	12.9%	0.30	890	110	12000	33.3	6667
C14	750	25	4500	12.9%	0.30	890	110	12000	33.3	6667
C15	750	25	4800	12.9%	0.30	890	110	12000	33.3	6667
C16	650	25	3900	14.8%	0.30	890	110	12000	33.3	6667
C17	700	25	3900	13.8%	0.30	890	110	12000	33.3	6667
C18	800	25	3900	12.1%	0.30	890	110	12000	33.3	6667
C19	850	25	3900	11.4%	0.30	890	110	12000	33.3	6667
C20	750	20	3900	10.4%	0.30	890	110	12000	33.3	6667
C21	750	22	3900	11.4%	0.30	890	110	12000	33.3	6667
C22	750	30	3900	15.4%	0.30	890	110	12000	33.3	6667
C23	750	25	3900	12.9%	0.20	890	110	12000	33.3	6667
C24	750	25	3900	12.9%	0.40	890	110	12000	33.3	6667
C25	750	25	3900	12.9%	0.50	890	110	12000	33.3	6667
C26	750	25	3900	12.9%	0.60	890	110	12000	33.3	6667
C27	750	25	3900	12.9%	0.30	890	110	8000	33.3	4444
C28	750	25	3900	12.9%	0.30	890	110	18000	33.3	10000
C29	750	25	3900	12.9%	0.30	890	110	5213.6	33.3	2896
C30	750	25	3900	12.9%	0.30	890	110	12000	16.7	1667
C31	750	25	3900	12.9%	0.30	890	110	12000	25.0	3750
C32	750	25	3900	12.9%	0.30	890	110	12000	41.7	10417
C33	750	25	3900	12.9%	0.30	890	110	12000	33.3	6667
C34	750	25	3900	12.9%	0.30	770	110	12000	33.3	6667
C35	750	25	3900	12.9%	0.30	690	110	12000	33.3	6667
C36	750	25	3900	12.9%	0.30	620	110	12000	33.3	6667

Note: B, t and L are the cross-sectional dimension, wall thickness and column height, respectively; α denotes the steel ratio; n is the axial compression ratio; f_y and f_{cu} are the steel strength and concrete strength, respectively; m is the vehicle weight; v is the impact velocity; and E is the impact energy.

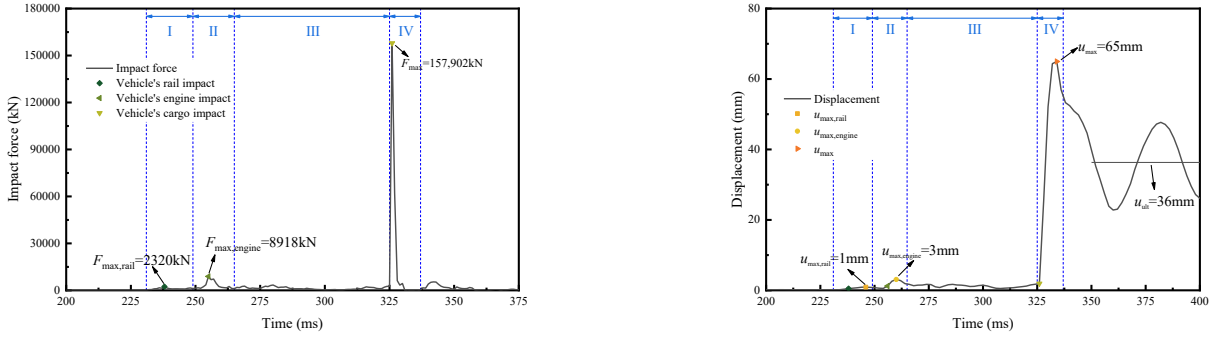

(a) Impact force

(b) Displacement

Fig. 4 Time-history curves

3.2. Development of bending moment

To analyze the damage evolution of the HCFHST columns, the bending moment development is examined in this section. Fig. 5(a) depicts the bending moment in the longitudinal direction at various characteristic points, where 'Max' and 'Min' denote the maximum and minimum value throughout the collision process. The maximum bending moment is 14,174 kN·m at a height of 3000 mm, denoted as M_{max}. In contrast, the minimum bending moment, M_{min}, is recorded at the bottom support, with a value of 15,091 kN·m. This indicates that the greatest bending moment appears at the bottom. As demonstrated in Fig. 5(a), the bending moment remains low, at only $0.15M_{min}$, during the bumper, engine, and cockpit impact stage. With the increase in displacement, the bending moment of the HCFHST column begins to stabilize. During the cargo impact stage, the bending moment gradually rises, ultimately reaching its maximum value.

The bending moment of the HCFHST column and the bending moments borne by each component at the M_{min} section are illustrated in Fig. 5(b). As exhibited in Fig. 5(b), the bending moment gradually increases to 1,520 kN·m during the bumper and engine impact stage, with the bending moment borne by the concrete increasing from 51% to 77% and the corresponding bearing proportion of steel tube decreasing from 49% to 23%. This phenomenon can be attributed to the overall stress of each component are relatively low, as discussed in Section 3.4. During the cockpit impact stage, the bending moment continues to rise, reaching 2,217 kN·m. The increased stress in the steel tube causes an increase in the bending moment, which grows to 29% of its initial value. Consequently, this results in a 6% decrease in the bending moment carried by the concrete. These analyses indicate that concrete is the key component carrying the bending moment during the bumper, engine, and cockpit impact stages. Consequently, the bending moment exhibited a gradual increase, attaining its maximum at 337 ms. Due to the concrete damage and the high stress in the steel tube, the bearing bending moment of the concrete has dropped to 2%, implying that the steel tube constitutes the main bending moment bearing component in the main displacement development stage. In summary, the HCFHST columns produced the greatest bending moment at the bottom under vehicle collisions. In the initial impact stage, concrete is the main component that bears the bending moment in the HCFHST column. Conversely, in the main displacement development stage, the steel tube becomes the critical component that bears the bending moment.

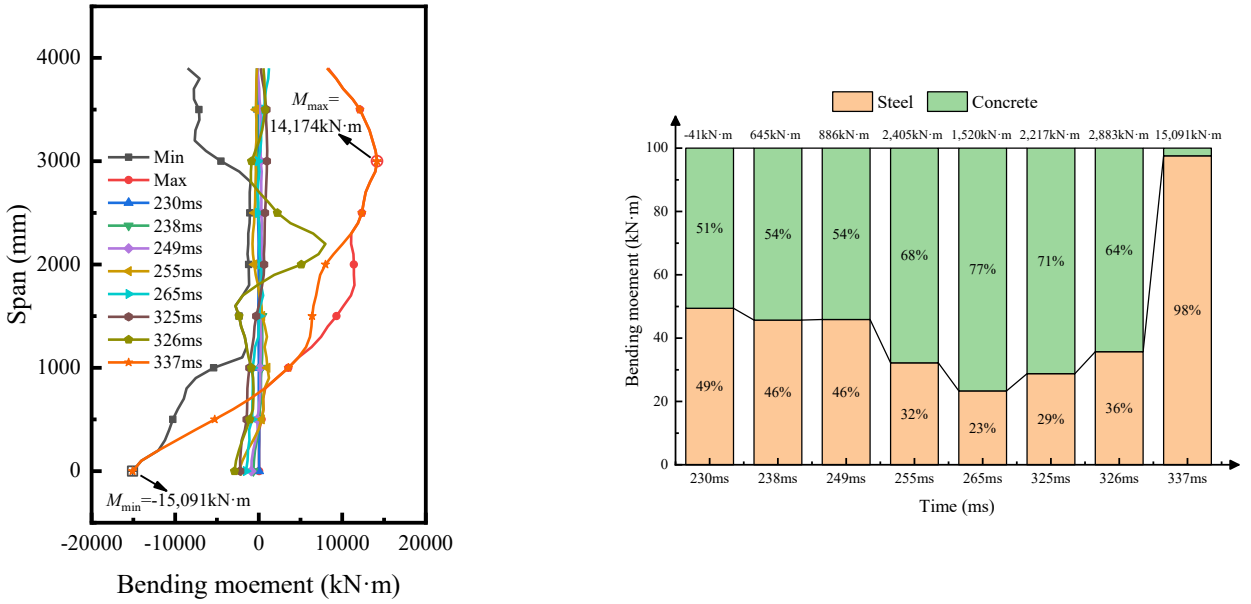

(a) Distribution of bending moment at each characteristic point

(b) Development of the bending moment at M_{min} section

Fig. 5 Development of bending moment of typical column

3.3. Development of shear force

To analyse the damage evolution of the HCFHST column, the shear force development of the HCFHST column is determined. Fig. 6(a) illustrates the shear force at various characteristic points along the longitudinal direction, where 'Max' and 'Min' mean the maximum and minimum shear forces observed during the collision process. The maximum shear force, S_{max}, is recorded at 44,647 kN, while the minimum shear force, S_{min}, is -29,725 kN, both occurring in the collision zone. This indicates that the greatest shear force is experienced in that specific area. As depicted in Fig. 6(a), it is observed that the shear force remains relatively low during the bumper impact, engine impact, and cockpit impact stages, reaching a value of $0.18S_{max}$. However, the shear force gradually increases and reaches its peak in the cargo impact stage.

Fig. 6(b) displays the shear force development of the HCFHST column and its components at the S_{max} section. As plotted in Fig. 6(b), the shear force fluctuates between -1555 kN and 513 kN during the bumper and engine impact stage, owing to low impact force, as explained in Section 3.1. In these stages, the steel tube bears more shear force than the concrete, implying that the steel tube is the critical components that bears the shear force. In the cockpit impact stage, the shear force fluctuates in the range of -1094~1078 kN. During this phase, the bearing shear force of the concrete exceeds that of the steel tube, suggesting that the concrete becomes the main shear force-bearing component. In the cargo impact stage, the maximum shear force reaches -44,647 kN at 326 ms, increasing the shear force bearing proportion of the steel tube to 15%, while the shear force borne by the concrete decreases to 85%. Following this peak, the shear force gradually declines. As the displacement progresses, the shear force carried by the concrete decreases. At 337 ms, the shear force had dropped to 5,560 kN, with the concrete only bearing 20% of the shear force. In contrast, the bearing shear force of the steel tube increased to 80%, indicating that the steel tube becomes the primary component to bear the shear force as the displacement progresses. In conclusion, the highest shear force occurs at the vehicle zone during a vehicle collision, and the steel tube is the main component bearing the shear force.

3.4. Evolution of damage

To examine the damage evolution of HCFHST columns during vehicle collisions, the stress development and effective plastic strain for each component of the HCFHST columns is analysed. Figs. 7 and 8 illustrate the stress and equivalent plastic strain of each component. These figures demonstrate that the HCFHST column undergoes bending deformation during a vehicle collision, with the maximum displacement occurring at the mid-span. During the first three impact stages, the Mises stress in the steel tube reaches $0.67f_y$, suggesting that only elastic deformation has occurred. In this phase, the concrete predominantly undergoes plastic deformation at the point of impact, with its principal stress increasing to $1.10f_{cu}$. Notably, 15% of the concrete in the mid-span section experiences plastic deformation. In the cargo impact stage, plastic deformation is displayed at the impact location on the front collision surface of the steel tube, while the concrete damage is mainly located at the impact location. After the vehicle collision is concluded, the maximum plastic deformation observed in the steel tube occurs at the mid-span section, particularly in the corner area, with a value of 0.099. The concrete in this section incurs complete damage. In summary, the HCFHST column exhibits bending deformation in response to the vehicle collision, with the most significant damage development occurring at the impact location.

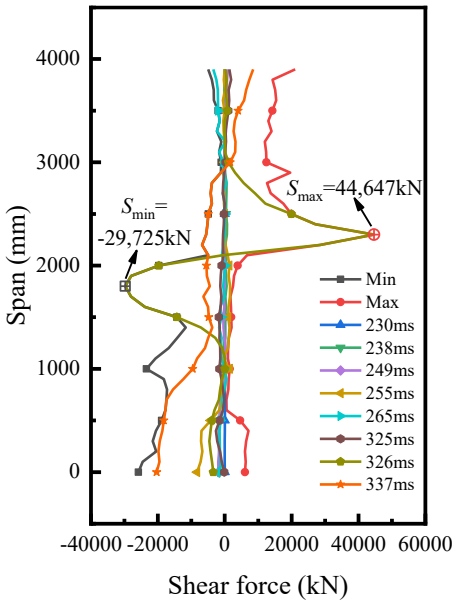

(a) Distribution of shear force at each characteristic point

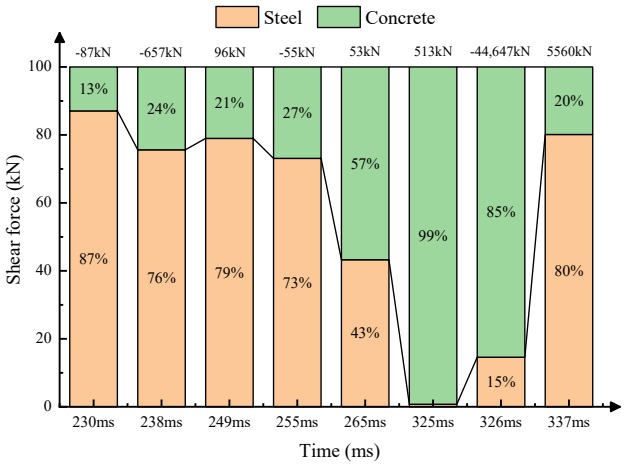

(b) Development of the shear force at S_{max} section

Fig. 6 Development of shear force of typical column

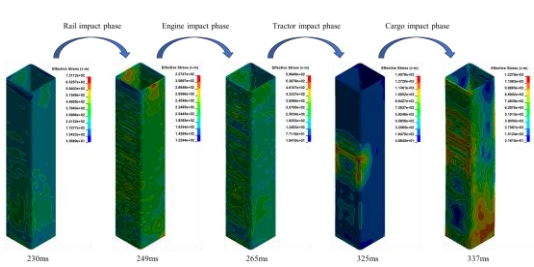

(a) Mises stress (unit: MPa)

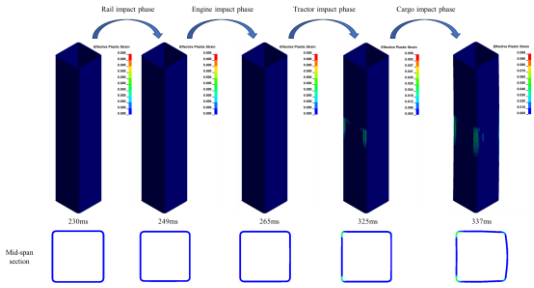

(b) Effective plastic strain

Fig. 7 Damage evolution of steel tube in typical column

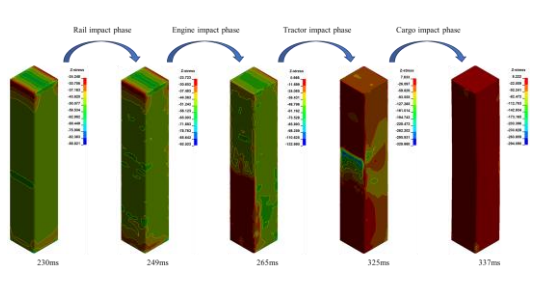

(a) Principle stress (unit: MPa)

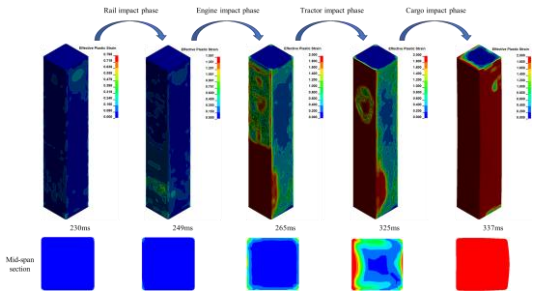

(b) Effective plastic strain

Fig. 8 Damage evolution of the concrete in typical column

3.5. Energy dissipating mechanism

Fig. 9 presents the time-history curves of energy and energy dissipated by each component. As illustrated in Fig. 9, the hourglass energy to the total energy (*TE*) ratio is less than 4%, confirming the reliability of the simulation. In the bumper, engine and cockpit impact stage, the dissipated energy of the HCFHST column is less than 0.010*TE*, whilst the energy dissipated by the vehicle can reach up to 0.217*TE*, indicating that the vehicle's deformation predominates in energy dissipation. In the cargo impact stage, the vehicle's kinetic energy rapidly decreases, with the HCFHST column dissipating 0.274*TE*. In this stage, the dissipated energy of concrete and steel tube is approximately 30% and 70%, respectively, indicating that the steel tube is the primary energy-dissipating component. Meanwhile, the vehicle's dissipated energy rises to 0.264*TE*. In summary, the HCFHST column dissipates less energy than the vehicle. The cargo impact stage is the primary energy-dissipating stage, with the steel tube playing a vital role in energy absorption.

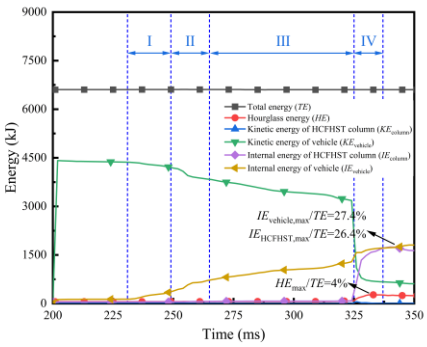

(a) Time-history curves of energy

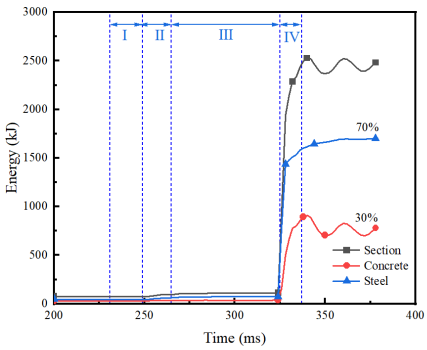

(b) Energy dissipation ratio of each component

Fig. 9 Development of energy

3.6. Parametric analysis

The effects of parameters on the anti-collision behaviours of HCFHST columns are investigated, and the detailed parameters and the corresponding simulation results are shown in Table 1. The impact of parameters on dissipated energy (E_{abs}), maximum displacement (u_{max}) and residual displacement (u_{ult}) of the HCFHST column is displayed in Figs. 10-12, respectively.

Changing sectional dimensions, steel tube thickness and material strength consequently changes the flexural strength and/or flexural stiffness of the HCFHST columns, affecting their dynamic behaviour during vehicle collisions. As demonstrated in Figs. 10-12, increasing the sectional dimension from 650 mm to 850 mm, the E_{abs} of the HCFHST column reduced from 2560 kJ to 2330 kJ, representing a 10% reduction. The u_{max} decreased from 73 mm to 58 mm, indicating a 26% drop, while the u_{ult} remained almost unchanged. This reduction in deformation and plastic energy dissipation is associated with the increase in sectional dimensions, which enhance the column's flexural strength and stiffness. When the steel tube thickness was increased from 20 mm to 30 mm, the E_{abs} by the columns rises from 2310 kJ to 2500 kJ, exhibiting a 10% increase. Additionally, the u_{max} reduces from 66 mm to 56 mm, indicating an 18% decrease, and the u_{ult} diminishes from 35 mm to 31 mm, showing a 13% reduction. These improvements are due to the thicker steel tube, the greater flexural strength and stiffness of the HCFHST column, thereby improving its anti-collision property. As the steel strength increases from 460 MPa to 890 MPa, the E_{abs} of the column reduces from 2600 kJ to 2460 kJ, representing a 6% decrease. Furthermore, the u_{max} reduces from 77 mm to 65 mm, indicating an 18% decrease, and the u_{ult} diminishes from 53 mm to 36 mm, showing a 47% reduction. It is evident that an increase in steel strength results in an enhancement of the flexural strength of the HCFHST column, leading to an increase in the impact resistance of the HCFHST column. When the concrete compressive strength is modified within the range of 60~120 MPa, the alterations in the E_{abs}, u_{max}, and u_{ult} of the column remain within 10%. This indicates that the effect of concrete compressive strength on the dynamic behaviour of the HCFHST column was negligible. To summarize, it can be concluded that the enhancement of the sectional dimension, the steel tube thickness, and the steel strength can lead to a substantial enhancement on the anti-collision performance of the HCFHST columns. Conversely, the concrete compression strength exerts a minor influence on the anti-collision performance of the HCFHST columns.

Increasing the column height, which raises the slenderness ratio, decreases the bending resistance of the HCFHST column. When the column height is increased from 3900 mm to 4800 mm, there is a minor influence on the energy dissipation. However, a slight increase is noted in the maximum and residual displacement, although this increase remains within 5%. Therefore, it can be concluded that the anti-collision properties of the HCFHST column diminish with increased column height. When the axial compression ratio rises from 0.2 to 0.6, the E_{abs} of the column increases from 2380 kJ to 2660 kJ, indicating an 11% enhancement. The increase in u_{max} and u_{ult} of the column also stays within 5%. As discussed in Section 3.4, the HCFHST column exhibits bending deformation during a vehicle collision. As a result, a higher axial compression ratio intensifies the second-order effect on the bending deformation of the column caused by the axial force, ultimately leading to a reduction in the anti-collision property of the HCFHST column.

The increase in impact mass from 5.2 tons to 18 tons led to a substantial rise in E_{abs}, which increased from 100 kJ to 5,040 kJ representing an addition of 49.4 times. The u_{max} rises from 4 mm to 95 mm, and the u_{ult} of the column exhibited an increase from 1 mm to 69 mm. Additionally, when the collision velocity rises from 16.67 m/s to 41.67 m/s, the E_{abs} also increased, from 322 kJ to 4,010 kJ, demonstrating an increment of 11.4 times. The maximum displacement grows from 18 mm to 82 mm, and the residual displacement of the column increases from 5 mm to 52 mm.

The slopes shown in Figs. 10-12 reveal the impact of each parameter on the dynamic behaviours of the HCFHST columns, ranked in descending order: vehicle weight, impact velocity, sectional dimension, steel tube thickness, steel strength, column height, axial compression ratio and concrete compressive strength. Consequently, it is recommended to enhance the anti-collision properties of HCFHST columns by raising the sectional dimension, steel tube thickness, or steel strength.

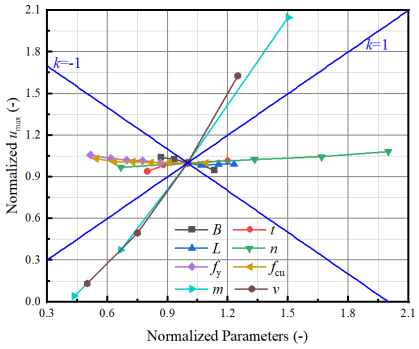

Fig. 10 Influence of parameters on the energy dissipation

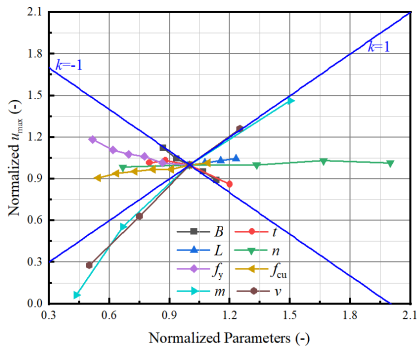

Fig. 11 Influence of parameters on the maximum displacement

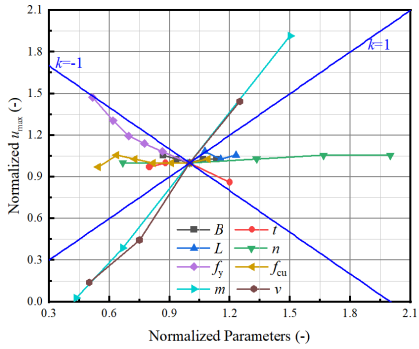

Fig. 12 Influence of parameters on the residual displacement

4. Calculation of maximum displacement

The literature has established a method for calculating the maximum displacement of a column under impact, based on the ideal elastic-plastic model and the equivalent SDOF method. This method assumes that the impactor's kinetic energy is fully converted into the column's internal energy. The formulas for calculating elastic displacements (X_e) and maximum displacements ($X_{m,impact}$) are presented in Eqs. (5) and (6), respectively. The main difference between this study and the findings in the literature [37] is that, in this paper, the vehicle's kinetic energy is not fully transformed into the HCFHST column's internal energy. Therefore, an energy dissipation formula for HCFHSTs column subjected to vehicle collisions is proposed. This formula will be incorporated into Eq. (6) to provide a more accurate calculation of the maximum displacement of the HCFHST column under vehicle collision.

$$X_e = \frac{F_y}{k} \tag{5}$$

$$X_{m,\text{impact}} = \frac{1}{2}\left[\frac{E_{impact}}{k_{\text{LM}}k(1+\alpha)} + X_e\right] \tag{6}$$

where, X_e denote the elastic displacement of the HCFHST column under vehicle collision; the bending resistance, F_y, can be determined as $F_y = \frac{8M_p}{L}$, where M_p is the flexural strength of the HCFHST column, and the calculation formulas detailed in reference [38]; the stiffness, k, can be calculated with $k = \frac{192EI}{L}$, where EI is the flexural stiffness of the column; $X_{m,impact}$ represents the maximum displacement of the column; k_{LM} is the uniformly distributed mass coefficient, which is 0.33 with a fixed-fixed boundary condition; E_{impact} denotes the impact energy; and α is the ratio of the HCFHST column mass to vehicle weight.

Key parameters are selected based on the parametric study in Section 3.6. The regression analysis is used to establish the relationship between the energy dissipation and key parameters, with the prediction formula in Eq. (7). Fig. 13(a) compares simulated and calculated energy dissipation, showing a mean of 1.005 and a SD of 0.031, with 92% of predicted values within a 5% error. These analyses verify that the formula can accurately and precisely predict the energy dissipation of the HCFHST columns. For maximum displacement, Eq. (7) can be substituted into E_{impact} in Eq. (6). Fig. 13(b) compares predicted and simulated maximum displacements, generating a mean of 0.893 and a SD of 0.203, with over 70% of predicted values within a 20% error. While the equivalent SDOF method may slightly underestimate the maximum displacement during vehicle collisions, the prediction accuracy remains acceptable within a 20% error range. Thus, using the energy dissipation formula with the equivalent SDOF method effectively predicts maximum displacement and provides useful guidance for engineering practice.

$$E_{abs} = 2460f(m)f(v)f(f_y)f(t)f(B)f(L) \tag{7}$$

where $f(m) = 0.00285m^2 + 0.0917m - 0.52$, unit in ton; $f(v) = 0.00095v^2 + 0.0045v - 0.21$, unit in m/s; $f(f_y) = 3.16 \times 10^{-7} \times {f_y}^2 - 0.00056f_y + 1.25$, unit in MPa; $f(t) = -0.00106t^2 + 0.0604t + 0.16$, unit in mm; $f(B) = -1.16 \times 10^{-6} \times B^2 + 0.0013B + 0.69$, unit in mm; and $f(L) = 4.54 \times 10^{-8} \times L^2 - 0.0004L + 1.87$, dimensionless.

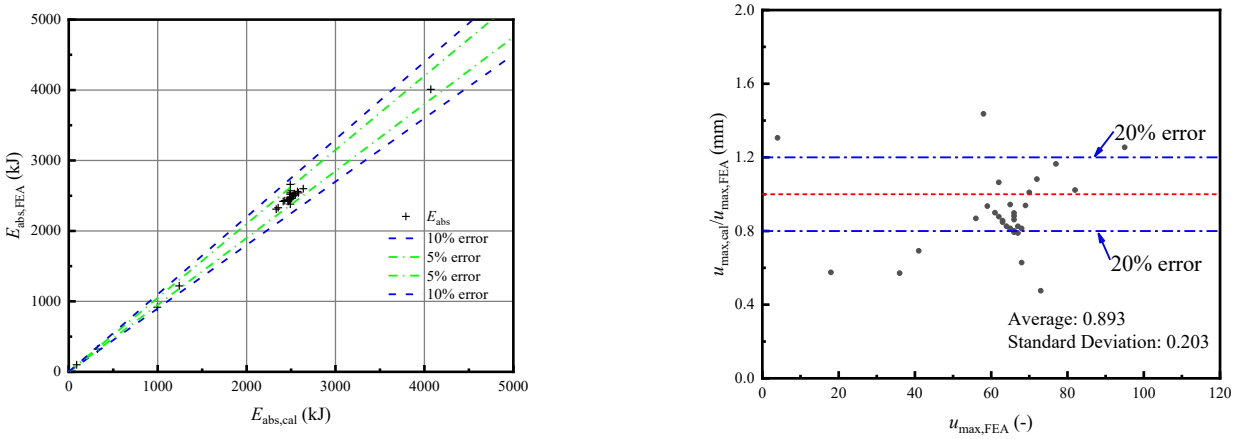

(a) Accuracy of energy dissipating calculation formula

(b) Accuracy of maximum displacement calculation formula

Fig. 13 Accuracy of calculation formula of energy dissipation and maximum displacement of HCFHST column under vehicle collision

5. Conclusions

This paper examines the dynamic performances of HCFHST columns under vehicle collision through numerical simulations. A thorough analysis of working mechanisms for the HCFHST column is conducted, covering the collision process, the development of internal forces, the evolution of damage, and the energy dissipation mechanisms. Through parametric analysis, the impact of parameters such as sectional dimensions, steel tube thickness, column height, axial compression ratio, material strength, vehicle weight and impact velocity on the impact resistance is investigated. Additionally, prediction equations for energy dissipation and maximum displacement of the full-scaled HCFHST columns under vehicle collisions are proposed. Based on the simulation results, the following conclusions can be concluded:

(1) The collected test data proves that the CS model and the CEB-FIP (2010) formula accurately reflect the dynamic performance of HSS and HSC under medium and high strain rate.

(2) The collision process can be categorised into four stages: bumper impact stage, engine impact stage, cockpit impact stage, and cargo impact stage. Among them, the cargo impact stage is the main dynamic behaviour stage of the column. Throughout the entire collision process, the HCFHST column exhibits a bending deformation. The HCFHST column dissipates energy lower than that of the vehicle, and the steel tube, dissipating 70% of the energy within the HCFHST column, is the main energy-dissipating component.

(3) Under a vehicle collision, the HCFHST column generates the greatest bending moment at the bottom and the greatest shear force at the vehicle impact zone. In the initial deformation stage, concrete is the critical internal force bearing component in the HCFHST column. As the displacement progresses, the steel tube takes over as the primary component bearing the internal force.

(4) The parametric results indicate that key factors influencing the dynamic performances of HCFHST columns include impact velocity, impact mass, sectional dimensions, steel tube thickness, and steel strength. Therefore, it is recommended to improve the anti-collision performance of HCFHST columns by raising the sectional dimensions, steel tube thickness, or steel strength.

Acknowledgements

This study is financially supported by the Key Program of National Natural Science Foundation of China, China (51938009), and the General Program of National Natural Science Foundation of China, China (51878419).

References

[1] BS 5400, Steel, concrete and composite bridges, Part 2: Specification for loads, British Standards Institution, London, 1988.
[2] AASHTO-LRFD, AASHTO-LRFD Bridge Design Specifications - Customary US Units, 6th edn, American Association of State Highway and Transportation Officials, Washington, 2020.
[3] BS EN 1991-1-7:2006, Eurocode 1: Actions on structures - Part 1-7: General actions - Accidental actions, European Committee for Standardization, Brussels, 2006.
[4] JGJ D60-2015, General Specification for Design of Highway Bridges and Culverts, China Communications Press, Beijing, 2015. (in Chinese).
[5] G.C. Li, B.W. Chen, Z.J. Yang, H.B. Ge, X. Li, AXIAL BEHAVIOR OF HIGH STRENGTH CONCRETE FILLEDHIGH STRENGTH SQUARE STEEL TUBULAR STUB COLUMNS, Adv Steel Constr 17(2) (2021) 158-168, https://doi.org/10.18057/IJASC.2021.17.2.6.
[6] L. H. Han, C. C. Hou, X. L. Zhao, K. J. Rasmussen, Behaviour of high-strength concrete filled steel tubes under transverse impact loading, J. Constr. Steel Res. 92 (2014) 25-39,

https://doi.org/10.1016/j.jcsr.2013.09.003.
[7] C. Hou, D. Wu, D. Ma, Experimental and numerical study on the impact performance of concrete-filled high-strength steel tube (CFHSST). Thin-Walled Structures 2024, 195:111450, doi:10.1016/j.tws.2023.111450.
[8] X. Yang, H. Yang, S. Zhang, Transverse impact behavior of high-strength concrete filled normal /high-strength square steel tube columns, Int. J. Impact Eng. 139 (2020) 103512, https://doi.org/10.1016/j.ijimpeng.2020.103512.
[9] X. Yang, Z. Zhang, Y. Zhu, W. Ma, J. Chen, D. Li, Dynamic responses and residual capacity of high-strength CFST members subjected to axial impact, J. Constr. Steel Res. 202 (2023) 107800, https://doi.org/10.1016/j.jcsr.2023.107800.
[10] G.C. Li, R.Z. Liu, C. Fang, X. Li, Dynamic responses of high-strength concrete-filled high-strength steel tubular column under lateral impact, J. Constr. Steel Res. 217 (2024) 108663, https://doi.org/10.1016/j.jcsr.2024.108663.
[11] D. Saini, B. Shafei, Performance of Concrete-Filled Steel Tube Bridge Columns Subjected to Vehicle Collision, J. Bridge Eng. 24 (8) (2019) 04019074, https://doi.org/10.1061/(ASCE)BE.1943-5592.0001439.
[12] M. Yu, X.X. Zha, Y.C. Wang, Behaviour of different types of columns under vehicle impact, Proceedings of the 3rd International Conference on Steel and Composite Structures, 2007, pp. 879-884. Manchester, UK.
[13] M. I. Alam, S. Fawzia, X.L. Zhao, Numerical investigation of CFRP strengthened full scale CFST columns subjected to vehicular impact, Eng. Struct. 126 (2016) 292-310, https://doi.org/10.1016/j.engstruct.2016.07.058.
[14] B. Hu, Y.Y. Liu, Vehicular Collision Performance Evaluation of Concrete-Filled Steel Tubular Piers Designed According to Current Codes in the US, Europe, and China, J. Build. Eng. 27 (6) (2022) 04022038, https://doi.org/10.1061/(ASCE)BE.1943-5592.0001889.
[15] B. Hu, H.B. Wang, Vehicular Impact Performance Evaluation Method for CFST Columns Based on Residual Deformation, Int. J. Steel Struct. 24 (2024) 529-549, https://doi.org/10.1007/s13296-024-00834-7.
[16] G.C. Li, B.W. Chen, B.W. Zhu, Z.J. Yang, H.B. Ge, Y.P. Liu, Axially loaded square concrete-filled steel tubular long columns made of high-strength materials: experimental investigation, analytical behavior and design, J. Build. Eng. 58 (2022) 104994, https://doi.org/10.1016/j.jobe.2022.104994.
[17] G.R. Cowper, P. S. Symonds, Strain Hardening and Strain Rate Effects in the Impact Loading of Cantilever Beams. Providence: Brown University, 1958.
[18] H. Yang, X. Yang, A. H. Varma, Y. Zhu, Strain-Rate Effect and Constitutive Models for Q550 High-Strength Structural Steel, Mater. Eng. Perform. 28 (2019) 6626-6637, https://doi.org/10.1007/s11665-019-04431-2.
[19] X. Yang, H. Yang, S. Zhang, Rate-dependent constitutive models of S690 high-strength structural steel, Constr. Build. Mater. 198 (2019) 597-607, https://doi.org/10.1016/j.conbuildmat.2018.11.285.
[20] X. Yang, H. Yang, Z. Lai, S. Zhang, Dynamic tensile behavior of S690 high-strength structural steel at intermediate strain rates, J. Constr. Steel Res. 168 (2020) 105961, https://doi.org/10.1016/j.jcsr.2020.105961.
[21] A.A. Alabi, P.L. Moore, L.C. Wrobel, J.C. Campbell, W. He, Tensile behaviour of S690QL and S960QL under high strain rate, J. Constr. Steel Res. 150 (2018) 570-580, https://doi.org/10.1016/j.jcsr.2018.08.009.
[22] E. Cadoni, D. Forni, Mechanical Behaviour of a Very-High Strength Steel (S960QL) under Extreme conditions of High Strain Rates and Elevated Temperatures, Fire Saf. J. 109 (2019) 102869, https://doi.org/10.1016/j.firesaf.2019.102869.
[23] Y. Zhu, H. Yang, S. Zhang, Dynamic Mechanical Behavior and Constitutive Models of S890 High-Strength Steel at Intermediate and High Strain Rates, J. Mater. Eng. Perform. 29 (2020) 6727–6739, https://doi.org/10.1007/s11665-020-05150-9.
[24] J.H. Kim, D. Kim, H. N. Han, F. Barlat, M.G. Lee, Strain rate dependent tensile behavior of advanced high strength steels: Experiment and constitutive modeling, Mater. Sci. Eng.A 559 (2013) 222-231, https://doi.org/10.1016/j.msea.2012.08.087.
[25] J. Yang, W. Hu, W.R. Wang, G. Shi, X.C. Wei, Relationship Between Strain Rate and Quasi-Static Tensile Behavior of 1000MPa DP Steel, Iron. Steel Res. Int. 23 (7) (2011) 39-42, https://doi.org/10.13228/j.boyuan.issn1001-0963.2011.07.006. (in Chinese)
[26] W. Wang, Y. Ma, M. Yang, P. Jiang, F. Yuan, X. Wu, Strain Rate Effect on Tensile Behavior for a High Specific Strength Steel: From Quasi-Static to Intermediate Strain Rates, METALS-BASEL 8 (1) (2018) 11, https://doi.org/10.3390/met8010011.
[27] J.S. Huo, X. Zeng, H.T. Wang, TENSILE BEHAVIOUR OF TMCP Q690D HIGH-STRENGTH STRUCTURAL STEEL AT STRAIN RATES FROM 0.00025 TO 760 S-1, Adv Steel Constr 18(1) (2022) 488-494, https://doi.org/10.18057/IJASC.2022.18.1.7.
[28] CEB-FIP. Model code 2010: first complete draft. Lausanne: Fédération Internationale du Béton, 2010.
[29] L. E. Malvern, C. A. Ross, Dynamic response of concrete and concrete structures, Second Annual Technical Report, AFOSR Contract No. F49620-83-K007 (1985).
[30] C. A. Ross, D. M. Jerome, J. W. Tedesco, M. L. Hughes, Moisture and Strain Rate Effects on Concrete Strength, Mater. J. 93 (3) (1996) 293-300, https://doi.org/10.14359/9814.
[31] Y.B. Guo, G.F. Gao, L. Jing, V.P.W. Shim, Response of high-strength concrete to dynamic compressive loading, Int. J. Impact Eng. 108 (2017) 114-135, https://doi.org/10.1016/j.ijimpeng.2017.04.015.
[32] T. Ngo, P. Mendis, A. Whittaker, A rate dependent stress-strain relationship model for normal, high and ultra-high strength concrete, Int. J. Prot. Struct. 4 (2013) 451-466, https://doi.org/10.1260/2041-4196.4.3.451.
[33] W. Wang, Z. Zhang, Q. Huo, X. Song, J. Yang, X. Yang, J. Wang, X. Wang, Dynamic Compressive Mechanical Properties of UR50 Ultra-Early-Strength Cement-Based Concrete Material under High Strain Rate on SHPB Test, Mater. 15 (17) (2022) 6154, https://doi.org/10.3390/ma15176154.
[34] Y.B. Guo, G.F. Gao, L. Jing, V.P.W. Shim, Quasi-static and dynamic splitting of high-strength concretes – tensile stress–strain response and effects of strain rate, Int. J. Impact Eng. 125 (2019) 188-211, https://doi.org/10.1016/j.ijimpeng.2018.11.012.
[35] H. Schuler, H. Hansson, Fracture behaviour of High Performance Concrete (HPC) investigated with a Hopkinson-Bar, J. Phys. IV France 134 (2006) 1145-1151, https://doi.org/10.1051/jp4:2006134175.
[36] J. Liu, W. Wang, K. He, D. Kong, X. Dai, X. Zhao, Dynamic tensile and stress wave transmitting characteristics of high strength and high ductility concrete, Constr. Build. Mater. 449 (2024) 138259, https://doi.org/10.1016/j.conbuildmat.2024.138259.
[37] M. Ali, J. Sun, N. Lam, L. Zhang, E. Gad, Simple hand calculation method for estimating deflection generated by the low velocity impact of a solid object, Aust. J. Struct. Eng. 15 (3) (2014) 243-259, http://dx.doi.org/10.7158/S13-006.2014.15.3.
[38] G.C. Li, B.W. Chen, Z.J. Yang, Y.H. Feng, Experimental and numerical behaviour of eccentrically loaded high strength concrete filled high strength square steel tube stub columns, Thin-Walled Struct. 127 (2018) 483–499, https://doi.org/10.1016/j.tws.2018.02.024.